Conduction mechanisms in Al-Ta_2O_5-Al_2O_3-Al rectifiers

A.D. Weerakkody, N. Sedghi, X. Zhan, I.Z. Mitrovic, S. Hall
Department of Electrical Engineering and Electronics,
University of Liverpool, Liverpool, L69 3GJ, UK

***Abstract* - This paper investigates the dominant conduction mechanisms in two bi-layer Ta_2O_5-Al_2O_3 structures fabricated by atomic layer deposition and rf sputtering. In depth experimental (electrical and optical) and theoretical analysis have been conducted to demonstrate the dominancy of quantum mechanical tunnelling, a desirable conduction mechanism for high-speed nanorectifier device operation.**

***Keywords*— Metal-insulator-insulator-metal, conduction mechanisms, Schottky emission, Direct tunnelling, Fowler-Nordheim tunnelling, Spectroscopic ellipsometry**

I. Introduction

Metal-insulator-metal (MIM) devices have applications as high-speed rectifiers in rectennas for THz energy harvesting [1-3]. In an MIM diode, the electrons flow through an insulating layer in the scale of a few nanometers. The devices with two dielectric layers, namely metal-insulator-insulator-metal (MIIM), benefit from resonant tunneling which serves to enhance the rectification by increasing the nonlinearity of the current-voltage (*IV*) characteristics [4,5]. These characteristics are achieved by the conduction mechanisms thermionic emission and quantum mechanical tunneling, however for less temperature dependent high-speed operation, the dominant conduction should be quantum tunneling. Based on this principle of operation, insulators with large electron affinities ($q\chi$) are desirable since they can produce small energy barriers at the metal electrodes and allow Fowler-Nordheim tunneling (FNT) to occur at small applied bias (low turn on voltage). Tantalum oxide (Ta_2O_5) with large $q\chi$ = 3.75 eV [6-8] appears to be a promising insulator for rectenna applications. However, in Ta_2O_5 layer FNT needs to dominate over emission based conduction mechanisms such as Poole-Frenkel (PF) and Schottky emission (SE). It has been reported recently that conduction in thick (10 nm) and thin (5 nm) Ta_2O_5-based MIM nanorectifiers is by electrode-limited SE in low bias regime and bulk-limited PF at larger bias [6], limiting their ultra-high frequency applications. A possible solution is to introduce nanolaminate bi-layers of Al_2O_3 and Ta_2O_5 [5], where transport in Al_2O_3 films has been found to be dominated by tunneling [5,7], while in Ta_2O_5 by PF emission. Overall rectifier performance in [5] has been found to be enhanced by a mechanism termed as "defect enhanced direct tunneling". This paper demonstrates two MIIM device structures with Al_2O_3 as the large barrier oxide, Ta_2O_5 as the small barrier oxide, and Al as electrodes. In-depth electrical characterization and theoretical analysis shows clearly dominance of tunneling in both insulator layers.

II. Device Fabrication And Experimental Details

MIIM devices were fabricated on cleaned 2.5 cm by 2.5 cm corning glass substrates. Atomic force microscopy (AFM) on cleaned substrate shows the average rms roughness of 0.32 nm. An aluminum layer with thickness of ~60 nm was deposited by thermal evaporation on the glass substrate to act as the bottom contact electrodes, patterned either by photolithography or a shadow mask. The average rms surface roughness after Al deposition was ~0.9 nm. The surface roughness of the substrate and the bottom metal contact was found to have a large impact on device performance in agreement with recent work [9]. Thin layers of 1 nm Al_2O_3 and 4 nm Ta_2O_5 were deposited either by atomic layer deposition (ALD) or rf magnetron sputtering. Finally Al top electrodes were defined either by photolithography or a shadow mask, at a deposition rate of 0.4 - 0.5 nm/s. The top view of photolithography mask illustrating bottom and top metal electrodes and actual MIIM device position is shown in Fig. 1a. The cross-sections of fabricated MIIM devices are shown in Figs. 1b and 1c, and refer to Al/Al native oxide/Ta_2O_5/Al labeled as MIIM-1 and Al/Al native oxide +1 nm Al_2O_3/Ta_2O_5/Al labeled as MIIM-2 respectively. Note that due to breaking vacuum immediately after bottom Al contact evaporation, there was an unintentional growth of native Al_2O_3 layer prior actual deposition of 1 nm Al_2O_3 by ALD or sputtering.

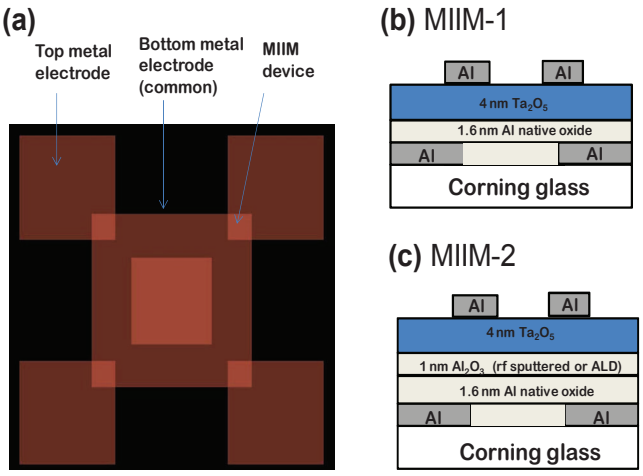

Fig. 1. (a) Photolithography mask used for MIIM device fabrication. The cross-sections of Al/Al_2O_3/Ta_2O_5/Al devices without (b) and (c) with intentionally deposited 1 nm Al_2O_3 layer.

978-1-4799-8229-5/151/$31.00 ©2015 IEEE

Variable angle spectroscopic ellipsometry (VASE) was performed on bulk Ta_2O_5 in order to extract the bandgap and the layer thickness. Subsequently, high temperature VASE measurements were performed to study the bandgap dependency with temperature. Room and temperature dependent *IV* measurements were performed in a dark probe station, using an Agilent B1500 semiconductor parameter analyzer.

III. Results And Discussion

Room and high temperature VASE measurements were performed on Ta_2O_5 deposited on a cleaned Si wafer to extract the optical properties, thickness and bandgap values within a wavelength range of 241.1 – 1686.7 nm (referring to energy range 0.7 to 5.2 eV) and at the angles 65^0, 70^0 and 75^0. CompleteEASE and WVASE 32 software programs were used to analyse the experimental (ψ, Δ) vs. photon energy data (Fig. 2a). Initially a theoretical model was developed to match the experimental data obtained on the Si reference sample. Then the Ta_2O_5 layer was superimposed to the reference model in order to extract the optical properties of Ta_2O_5 (see Figs. 2b-c). A band gap of ~4.5 eV was extracted by extrapolating the leading edge of absorption coefficient vs photon energy curve in Fig. 2d. The value is consistent to recently reported in [7].

Temperature dependent VASE analysis was performed on bulk Ta_2O_5 and it was evident that the band gap values were reduced by ~0.08 eV (Fig. 2d) over the temperature range of 298 K to 348 K.

The current density vs voltage (*JV*) characteristics for MIIM-1 and MIIM-2 type of devices are shown in Figs. 3a and 3b respectively. In-depth analysis for Poole-Frenkel and Schottky emission were carried out in order to investigate the dominant conduction mechanism, at fields below 2.5 $MVcm^{-1}$, where Ta_2O_5 is the current limiting layer. Both MIIM-1 and MIIM-2 devices are double dielectric due to the formation of Al native oxide or intentional deposition of Al_2O_3. It has been shown that tunnelling is a dominant mechanism in Al_2O_3 layer [7], hence conduction in Ta_2O_5 was considered as the main objective of this work. The relative dynamic permittivity extracted from the PF plots over the electric field range of 0-2.5 $MVcm^{-1}$ shown in Fig. 4, ranged from 25.6 to 39 for MIIM-1, and 11.9 to 14.5 for MIIM-2 structures. The dielectric constant associated with PF is expected to have the high frequency value as emission of electrons from the traps should occur at times corresponding to optical frequencies. The optical permittivity (n^2) was estimated to be ~4.5 at the wavelength of 580 nm from VASE (Fig. 2c); therefore from 0-2.5 $MVcm^{-1}$ PF in Ta_2O_5 is excluded as the dominant conduction mechanism in these devices. Alimardani *et al.* have reported a relative dynamic permittivity of 4.6 $\pm$ 0.1 by similar analysis [6].

Schottky emission analysis was performed on both devices and the dynamic permittivity was extracted from the Schottky plots shown in Fig. 5. The dynamic permittivity of Ta_2O_5 layer for MIIM-1 structure (Fig. 5a) varied from 5.1 to 2.6 with the increase in temperature from 293 K to 373 K.

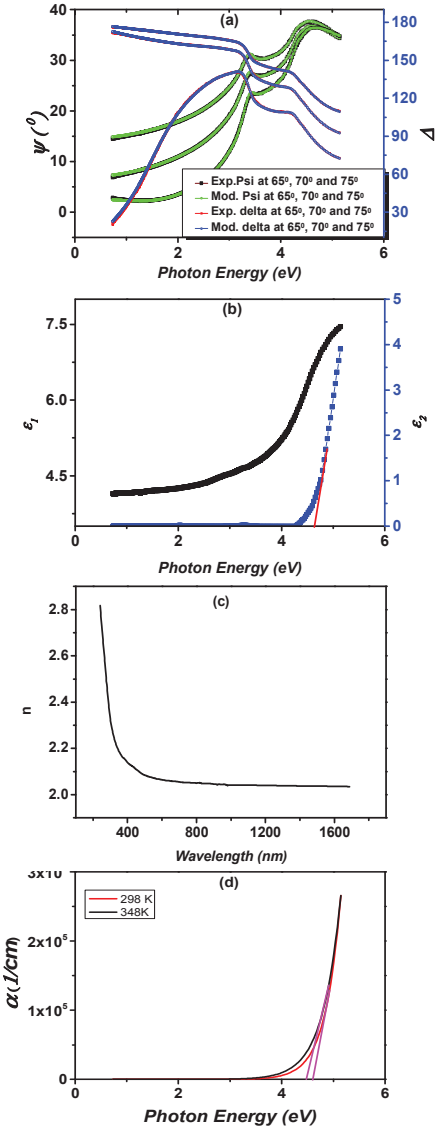

Fig. 2. (a) Experimental and modelled ψ and Δ angles vs photon energy (E), (b) real and imaginary parts of relative dynamic permittivity vs E, (c) refractive index vs wavelength, and (d) temperature dependence of absorption coefficient (α) vs E on bulk (20 nm) Ta_2O_5. layer.

The room temperature dynamic permittivity (K_r) value is comparable to the optical dynamic permittivity extracted from VASE, which is ~4.5; however the dynamic permittivity extracted on the MIIM-2 structure ranged from 2.5 to 1.7 over the same temperature range. Schottky barrier height was extracted from Arrhenius plots in Fig. 6 and the extracted values for the MIIM-1 structure (Fig. 6a) ranged from 0.66 eV to 1.08 eV with the increase in electric field from 1.25 $MVcm^{-1}$ to 5 $MVcm^{-1}$ respectively. This could be due to the presence of both tunneling and SE at low electric fields (< 2.5 $MVcm^{-1}$). However with the increase of field tunnelling becomes superior, hence the barrier height extracted from Schottky analysis increases significantly. The barrier heights calculated for the MIIM-2 structure (Fig. 6b) have values ranged between 0.44 eV to 0.35 eV with the increase in electric field from 1 $MVcm^{-1}$ to 4 $MVcm^{-1}$. It should be noted that the barrier height

calculated at lower field is closer to the expected value due to smaller influence of tunnelling.

Theoretical approximations for tunneling and thermionic emission were considered and compared with the experimental results on Ta_2O_5 layer. The dynamic permittivity and the barrier height extracted from fitting the experimental results to Schottky conduction were used while estimating the current density theoretically. Direct tunneling (DT) and Fowler-Nordheim currents were calculated for different barrier heights at the Al/Ta_2O_5 interface as shown in Fig. 7.

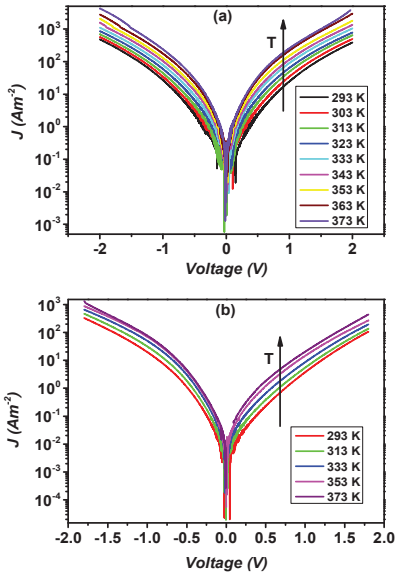

Fig. 3. Temperature dependent *JV* plots of (a) MIIM-1 and (b) MIIM-2 devices (Device area is A = 10^{-8} m^2).

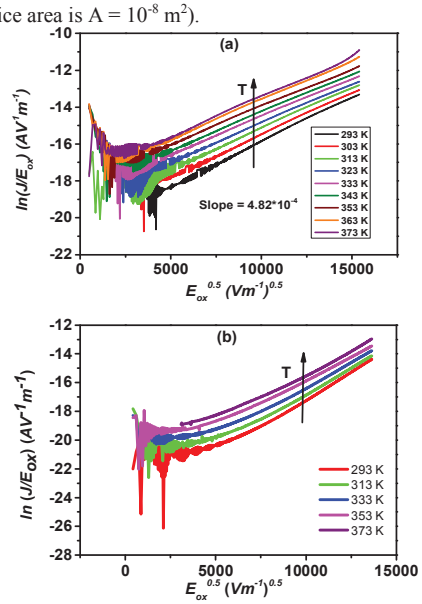

Fig. 4. Temperature dependent PF plots of (a) MIIM-1, and (b) MIIM-2 devices (A = 10^{-8} m^2).

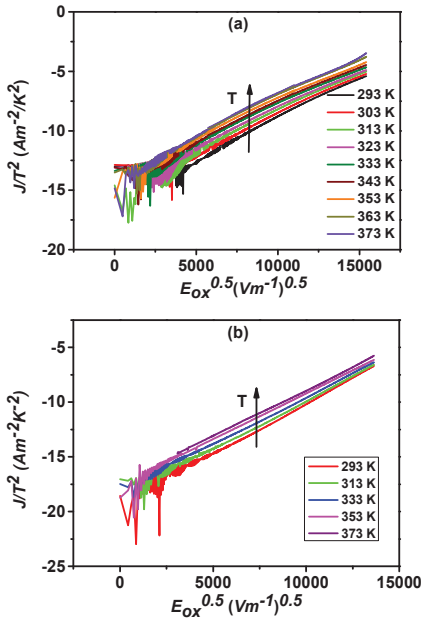

Fig. 5. Temperature dependent Schottky plots of (a) MIIM-1 and (b) MIIM-2 devices (A = 10^{-8} m^2).

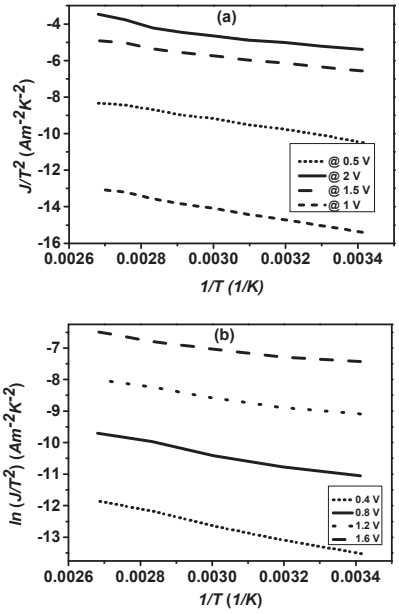

Fig. 6. Arrhenius plots for Schottky emission conduction for (a) MIIM-1 and (b) MIIM-2 devices (A = 10^{-8} m^2).

The experimentally obtained currents for the MIIM-1 structure are one to two orders of magnitude smaller than the theoretically estimated current using the SE equation with barrier height of 0.66 eV (Fig. 7a). The extracted barrier heights at different electric fields were applied to the SE equation and this lead to observe a significant difference in theoretical currents in contrast to the experimentally obtained current in Fig. 7a. Nevertheless direct tunneling with a barrier height of 0.7 eV at the Al/Ta_2O_5 was comparable to the experimental currents at lower electric fields (0 – 2.5 $MVcm^{-1}$). The thick Al_2O_3 limits the current in MIIM-2 structure even at lower electric fields (<1.5 $MVcm^{-1}$) and also it is evident that the theoretically calculated current levels using Schottky

equation are significantly larger than the experimentally obtained current levels.

Determining the dominant conduction mechanism in a bi-layer device is not straightforward. However, the conduction in thin Al_2O_3 (< 3 nm) in this range of electric field (0 – 5 $MVcm^{-1}$) is always direct tunneling [5]. This is experimentally proven by temperature independence of current in Al_2O_3 (ZCAN/Al_2O_3/Al) [7]. It is evident that the experimental *JV* characteristics (Fig. 3) are temperature dependent; therefore they were compared against the PF and SE conductions assuming the conduction in Ta_2O_5 dominated by either PF or SE. Ta_2O_5 is the current limiting layer at low fields (<2.5 $MVcm^{-1}$), presumably the conduction in Ta_2O_5 layer at electric fields < 2.5 $MVcm^{-1}$ could be a combination of SE and DT and changing to FN at fields ≥ 3.5 $MVcm^{-1}$ [10]. Presence of PF can be excluded due to the large values extracted for the dynamic permittivity. At electric fields ≥ 2.5 $MVcm^{-1}$, the Al_2O_3 is limiting the current by DT on both polarities. A possible reason for the change in current at high fields with the increase in temperature could be due to increased current levels at lower fields as a result of SE; hence it follows the same trend.

Alimardhani *et al* [5,6] have reported that conduction is dominated by SE at low electric fields and PF at large electric fields on a ZCAN/ (5 nm and 10 nm) Ta_2O_5/Al MIM structures, however, the MIIM structure ZCAN/ 2.5 nm Al_2O_3/2.5 nm Ta_2O_5 demonstrated negligible temperature dependence, characteristic of tunneling. In this work, we observe no evidence of PF in 4 nm Ta_2O_5/1.6 to 2.6 nm Al_2O_3 bi-layer devices, which indicates high-quality deposited structures. The presence of native Al_2O_3 layer shows no detrimental effect on conduction however it can shift the onset of resonant tunnelling to higher voltages [10], limiting device use for THz energy harvesting applications.

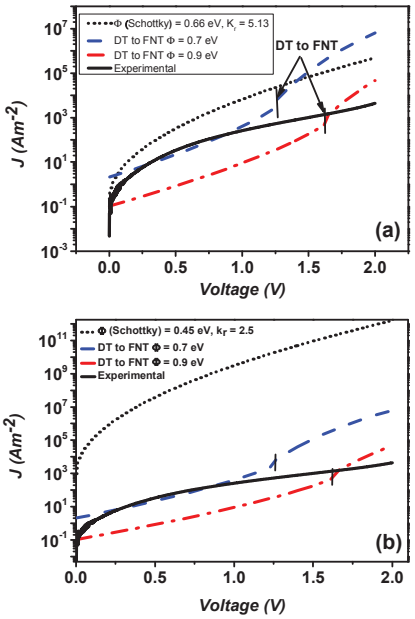

Fig. 7. Experimental and calculated *JV* plots (DT, FNT and SE) for (a) MIIM-1 and (b) MIIM-2 devices.

IV. Conclusion

This paper experimentally and theoretically demonstrates the dominance of certain conduction mechanisms on the ALD and rf sputtered nanometer scale bilayer Ta_2O_5/Al_2O_3 structures. Poole-Frenkel is excluded as a dominant conduction mechanism due to the large difference between the dynamic permittivity values extracted from the PF plots measured by VASE. The conduction could be a combination of Schottky emission and quantum mechanical tunneling in Ta_2O_5 based on the experimental results and theoretical calculations. The fabricated Ta_2O_5/Al_2O_3 nanostructures show promising properties for use in future high-speed nanorectifiers.

Acknowledgments

The work has been funded by EPSRC, UK, under project EP/K018930/1. ALD material deposition was done by J. Wrench and P. Chalker. R. Treharne, L. Phillips, and K. Durose are acknowledged for sputtering of insulator layers.

References

[1] M.N. Gadalla, M. Abdel-Rahman and A. Shamim, "Design, Optimization and Fabrication of a 28.3 THz Nano-Rectenna for Infrared Detection and Rectification", Scientific Reports, vol. 4, pp. 4270-1-9, 2014.

[2] S. Grover and G. Moddel, "Applicability of Metal/Insulator/Metal (MIM) Diodes to Solar Rectennas", IEEE Journal of Photovoltaics, vol. 1, no. 1, pp. 78-83, 2011.

[3] S. Krishnan, E. Stefanakos, and S. Bhansali, "Effects of dielectric thickness and contact area on current-voltage characteristics of thin film metal-insulator-metal diodes", Thin Solid Films, vol. 516, pp. 2244-2250, 2008.

[4] S. Grover and G. Moddel, "Engineering the current–voltage characteristics of metal–insulator–metal diodes using double-insulator tunnel barriers", Solid-State Electronics, vol. 67, pp 94-99, 2012.

[5] N. Alimardani and J.F. Conley Jr., "Enhancing metal-insulator-insulator-metal tunnel diodes via defect enhanced direct tunnelling", Applied Physics Letters, vol. 105, pp. 082902-1 – 082902-5, 2014.

[6] N. Alimardani, J. McGlone, J.F. Wager, and J.F. Conley Jr., "Conduction process in metal-insulator-metal diodes with Ta_2O_5 and Nb_2O_5 insulators deposited by Atomic Layer Deposition", J. Vac. Sci. and Tech. A, vol. 32, pp. 01A122-1 - 01A122-6, 2014.

[7] N. Alimardani, S. W. King, B. L. French, C. Tan, B. P. Lampert, J. F. Conley Jr., "Investigation of the impact of insulator material on the performance of dissimilar electrode metal-insulator-metal diodes", J. Appl. Phys., vol. 116, pp. 024508-1 – 024508-11, 2014.

[8] B.C. Lai and J Y. Lee, "Leakage current mechanism of metal-Ta_2O_5-metal capacitors for memory device applications", Journal of the Electrochemical Society, vol. 146, no. 1, pp. 266-269, 1999.

[9] N. Alimardani, E.W. Cowell III, J.F. Wager, J.F. Conley Jr, D.R. Evans, M. Chin, S.J. Kilpatrick, and M. Dubey, "Impact of electrode roughness on metal-insulator-metal tunnel diodes with atomic layer deposited Al_2O_3 tunnel barriers", Journal of Vacuum Science and Technology A, vol. 30, no. 1, pp. 01A113-1 – 01A113-5, 2012.

[10] A. D. Weerakkody, N. Sedghi, I.Z. Mitrovic, H. van Zalinge, I. Nemr Noureddine, S. Hall, J.S. Wrench, P.R. Chalker, L.J. Phillips, R. Treharne, K. Durose, "Enhanced low voltage nonlinearity in resonant tunneling metal-insulator-insulator-metal nanostructures", Microelectronic Engineering, March 2015 (in press).